Annals of Glaciology 32 2001

Particle densities, velocities and size distributions in large avalanches from impact-sensor measurements

Mark Schaer, Dieter Issler*
Eidgenössisches Institut für Schnee- und Lawinenforschung (SLF), CH-7260 Davos Dorf, Switzerland

ABSTRACT. In winter 1998/99, high-frequency pressure measurements with 10 cm sensors mounted 1–19 m above ground were carried out in the upper run-out zone of the avalanche test site at Vallée de la Sionne, Switzerland. Two large dry-snow avalanches clearly revealed a three-layered structure, with surprisingly low pressures in the suspension (or powder-snow) layer. The height of the saltation layer varied between 1 and > 3 m. From the duration, impulse and frequency of single-particle impacts (observed in the saltation layer and intermittently in the dense flow), particle-size and velocity distribution functions as well as strongly varying saltation-layer densities were found. With improved methods for peak detection and correction for grazing impacts, pressure measurements will become a premier tool for testing granular flow models.

1. CURRENT KNOWLEDGE OF AVALANCHE STRUCTURE

The demand for ever more precise avalanche-hazard mapping entails the need for more detailed knowledge of the physical processes within the different types of avalanches. It is widely accepted that changes in the flow regime may occur during an avalanche event and that they may greatly influence, for example, the effective friction of the flow and thus the run-out distance and the impact pressures. Approaches based on granular theory hold promise, but require much more detailed data from within real avalanches. Note also that realistic models of snow entrainment and deposition can only be developed if the structure of the flow is correctly described by the flow model.

Earlier studies of avalanche structure, applying load cells and additional experimental techniques (Schaerer and Salway, 1980; Norem and others, 1985; Nishimura and others, 1987; Kawada and others, 1989; Nishimura and others, 1993), discovered the three-layered structure of dry-snow avalanches with a dense flow at the bottom, a "saltation" layer in the middle and the "powder-snow cloud" (suspension layer) on top. Velocity profiles (from cross-correlations between neighboring radars or photo cells) have been obtained only for a few events and only in the dense-flow layer (Gubler and others, 1986; Dent and others, 1998); they show a thin, strongly sheared bottom layer with a plug flow above it. So far, capacitance-sensor arrays (Dent and others, 1998) represent the only currently viable technique for measuring density profiles.

In this paper we show that small load cells with high time resolution allow analysis of single-particle impacts. From the particle momentum and impact duration, the size and velocity are found if the particle density is known (from a posteriori field investigations). Classifying impacts within short time intervals, the time evolution of size and velocity distributions at different heights can be obtained. The analysis proves much more involved than the usual pressure measurements, however. Identifying single particles within swarms of impacts is a difficult task, and significant corrections have to be made for excentric collisions of large particles. Our goal is merely to demonstrate the potential of the approach; the present analysis is far from exhaustive and will need refinement.

We use data from a slow wet-snow avalanche and two large dry-snow avalanches, collected at SLF's Vallée de la Sionne test site, Switzerland (Ammann, 1999; Issler, 1999), in the course of the exceptional winter 1998/99 (Dufour and others, unpublished). A related paper reports on measurements of the global mass balance (Vallet and others, 2001).

2. EXPERIMENTAL SET-UP

The two principal release zones of the Crêta Besse path are located at 2400–2700 m a.s.l. Between 2050 and 1800 m a.s.l., avalanches are quite strongly channeled in one or two gullies. The upper run-out zone extends from about 1800 m a.s.l. to the Sionne river at 1450 m a.s.l. for slow avalanches. Large avalanches will not decelerate appreciably before reaching the river; the dense flow avalanche (DFA) follows the river, and the powder-snow avalanche (PSA) may climb a large distance on the steep opposite slope, on which a reinforced-concrete shelter houses the crew and the Doppler radars.

In the upper run-out zone, at 1630 m a.s.l., several instrumented structures were built, among them a narrow, 5 m high steel wedge and a 20 m high tubular mast. Piezoelectric load cells were mounted 0.9, 2.1, 3.0 and 3.9 m, and 7 and 19 m above ground, respectively. Their active surface is 10 cm in diameter, and the lowest eigenfrequency is > 5 kHz; the pre-amplified signals are sampled at 15 kHz. In order to compensate for vibrations of the supporting structure, pairs of sensors were mounted in line on the tubular mast and at the uppermost position on the wedge, with only the front sensor exposed to the avalanche. Compensation was not

* Present address: NaDesCoR, Promenade 153, CH-7260 Davos Dorf, Switzerland.

https://doi.org/10.3189/172756401781819409 Published online by Cambridge University Press

Table 1. Characteristic properties of studied avalanche events

	12 December 1998	*30 January 1999*	*10 February 1999*
Main gully	South	North	South
Initial mass (t)	1500–3000	20 000	50 000
Snow humidity	Wet	Dry, cold	Dry, cold
Erosion at 1900 m ($kg\,m^{-2}$)		≈ 300	≥ 300
Front velocity at wedge ($m\,s^{-1}$)	3–5	50	60
Flow depth at wedge (m)	0.5–1.2	0.5–1.5	1.0–1.8
Height of PSA at wedge (m)	no PSA	20–30	≈ 50

Note: Approximate flow depth (from FMCW radar) is given for the dense-flow part only.

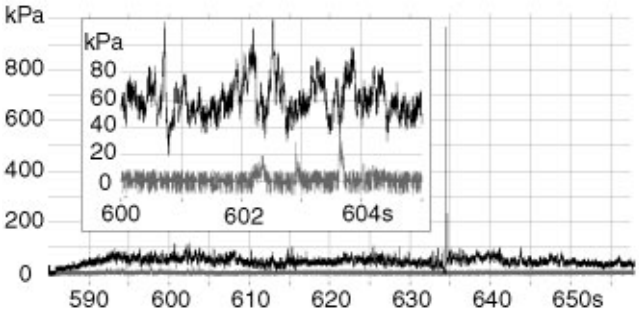

Fig. 1. Pressure measurements at wedge, avalanche of 12 December 1998. Black line: sensor 0.9 m above ground; gray line: sensor 2.1 m above ground.

necessary on the wedge, but was essential on the mast. For various reasons, a numerical low-pass filter set at 2 kHz was applied in the present analysis.

In the course of data analysis, a few problems in the raw data required special attention. Some sensors showed a pronounced drift during measurements, probably due to condensing humidity in the pre-amplifiers. Thanks to intermittent periods with virtually no impacts, the drift could be manually corrected almost everywhere. Furthermore, sudden large jumps of the signal level are sometimes observed during periods with high impact rates; the most likely explanation is that the impact shocks loosened the plugged connections between sensors and charge amplifiers. On 10 February 1999 the sensor at 7 m failed after about 4 s. Finally, construction equipment dangling from the top of the tubular mast caused regularly occurring noise.

3. RAW DATA: OVERVIEW AND MAIN CHARACTERISTICS

Table 1 summarizes the main characteristics of the events analyzed in this paper. Figure 1 shows the pressure measurement obtained from a very slow wet avalanche at the wedge on 12 December 1998. The deposits consisted of small to very large, refrozen "snowballs", the larger ones themselves consisting of conglomerates of smaller particles. The towering peak 48 s after avalanche arrival almost certainly is due to impact of a large stone. Before the event, the snow cover was about 0.4 m deep. The lowest sensor records a moderately fluctuating signal until the maximum recording time is reached. Sliding-window averages range from 30 to 70 kPa at the lowest sensor 0.9 m above ground. At 2.1 m, only occasional peaks of 20–30 ms duration are recorded; the sensors above show no signal at all. Consistent with this, the frequency-modulated continuous wave (FMCW) radars just 5 and 15 m upstream of the wedge indicate flow depths 0.8–1.3 m above a remaining snow cover of <0.5 m. Several methods for determining the avalanche front speed consistently arrive at values of 3–5 $m\,s^{-1}$. Note that even with an assumed density of 500 $kg\,m^{-3}$ the expected pressure $\mathcal{O}(\rho u^2)$ would only be about 10 kPa. A possible explanation of this discrepancy is discussed in section 4.

The data of 30 January 1999 present a radically different picture (Fig. 2). Except for a small peak about 20 s later, the avalanche passes the wedge in 5–6 s and the tubular mast in an even shorter interval. At 3 m above ground, a strongly fluctuating signal is recorded, with a quasi-static component (duration $\geq$1 s) up to 80 kPa, many peaks in the 200–400 kPa range and just a few very strong peaks up to 1200 kPa. Interestingly, the strong peaks last <10 ms, while the lesser ones last up to 50 ms and show smaller fluctuations lasting 5–20 ms. But already at 3.9 m above ground, significant pressures of 20–150 kPa occur only during about 2 s. Peaks of 5–10 ms exhibit fluctuations reaching 10–100% of the mean peak value and lasting 2 ms or less. As in the strongest peaks at 3.0 m, many spikes show skew: the pressure rises very rapidly to the maximum, then drops again more slowly.

Pressures at the tubular tower have a poorer signal-to-noise ratio because the signals were weaker than expected and were only a small percentage of the measurement range. Quasi-periodically occurring peaks at 2 Hz are due to the dangling construction equipment. Again, significant quasi-static pressures are recorded only during 2–3 s and are of the order of 4 kPa at 7 m and <1 kPa at 19 m. Superimposed peaks are in the range 5–15 kPa at 7 m and much less at 19 m; typical durations are 3–7 ms. Note the small, quasi-regular high-frequency fluctuations attributed to some eigenmode of the mast, and the symmetry of the peaks.

On 10 February 1999 many of the same characteristics are found again: at the wedge, asymmetric impact peaks (many of them very strong), in contrast to much more symmetric pressure fluctuations at 19 m on the mast. Several differences are conspicuous, however. The avalanche passage lasted about 30 s instead of 6 s, and typical impacts were recorded even at 7 m above ground (approximately 5 m above the sliding surface) during passage of the head. At 3.0 m quasi-static pressure up to 500 kPa persists over almost 30 s, rising continually during the first 20 s and then dropping slowly. Distinct impacts clearly dominate at 3.9 m, but they are strongest and most frequent as the head passes by; surprisingly, significant signals last only about 13 s, whereas the nearby FMCW radars recorded particles at that height during the entire time of passage.

The tubular mast at 19.0 m above ground recorded very low pressures in the powder-snow cloud: rarely >1 kPa. From the measured front velocities and very rough density estimates, pressures of at least 5 kPa were expected for the 10 February 1999 event. The quasi-static stagnation pressure should be even larger at 7 m, but instead pressure is observed to drop to near zero between impacts. Two possible elements of an explanation might be (i) strongly reduced velocities at the top of the PSA due to recirculation of snow–air mixture, and (ii) formation of a snow cone on the sensor, leading to a much smaller effective drag coefficient. Complementary measurement techniques are required to shed light on this question.

https://doi.org/10.3189/172756401781819409 Published online by Cambridge University Press

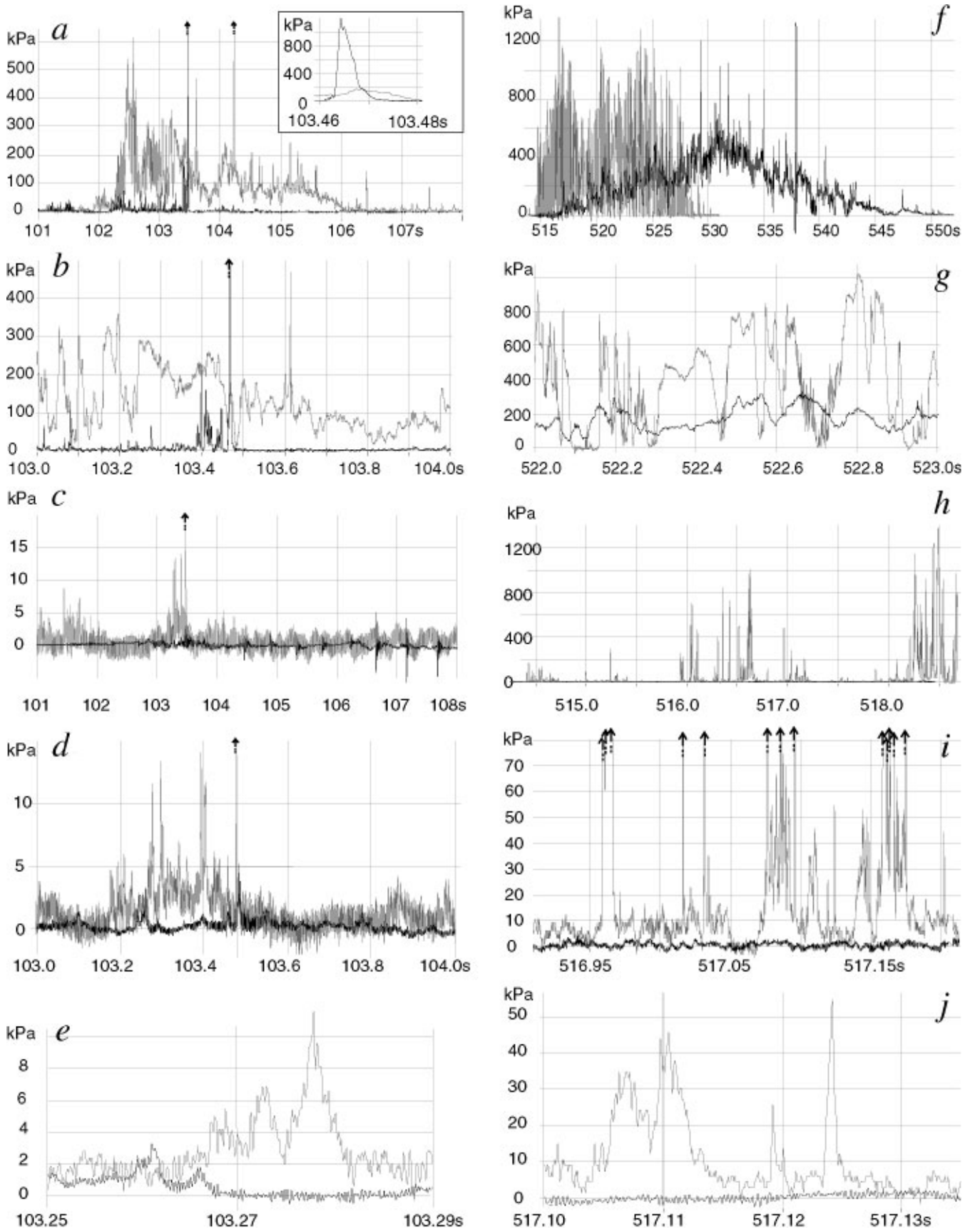

Fig. 2. Pressure measurements at wedge and tubular mast, avalanches of 30 January 1999 (left column) and 10 February 1999 (right column). (a, f) Raw data from sensors at 3.0 m (gray lines in (a), black lines in (f)) and 3.9 m (black lines in (a), gray lines in (f)) on wedge (lower sensors were inside snow cover). (b, g) Detail view of wedge measurements. (c, h) Filtered data from tubular mast at 7.0 m (gray lines) and 19.0 m (black lines). (d, e, i, j) Enlarged views of data from mast.

https://doi.org/10.3189/172756401781819409 Published online by Cambridge University Press

4. ANALYSIS METHOD FOR PARTICLE IMPACTS

Data analysis proceeds in the following steps, which will be explained in more detail below:

1. Peak detection on the low-pass filtered data; discrimination between single-particle impacts and particle clusters.
2. Determination of apparent particle size d' and velocity u' for each single-particle impact.
3. Classification of impacts within short intervals (0.25–1.5 s) with respect to d' and u', leading to the apparent impact distribution functions $\tilde{N}_{ij}(t)$ for size class i and velocity class j for each sensor.
4. Correction for distortion of the impact distribution functions due to excentric impacts of particles.
5. Extraction of partial densities for size and velocity classes.
6. Estimate of total avalanche density from total pressure on sensor, using the average velocity of single-particle impacts.

Peak detection

The raw data were first filtered with a low-pass Butterworth filter set at 2 kHz, and the noise level was determined. The criterion for a peak was a local minimum–local maximum–local minimum sequence where both minima are above a selected threshold, and pressure at the local maximum is at least 1.5 times larger than at either minimum. Each peak was extrapolated down to the noise level and subtracted from the signal before the next peak was searched for; this procedure allows detection of overlapping impacts if they are not too close. In the next step, multi-particle impacts (peaks with ripples, a flat top or of very long duration) that had not been resolved by the detection algorithm were eliminated. For each remaining impact, its initial time, duration τ and impulse I (integral of the force on the sensor over impact time) were registered.

Particle–sensor interactions for small particles

An adequate understanding of the complicated impact processes is essential to correct interpretation of the load-cell signals. Snow particles behave as a plastic material in this situation and are typically compressed from their original density $\rho^{(p)} \approx 300$–$400\,\mathrm{kg\,m^{-3}}$ to $\rho^{(c)} \approx 500$–$650\,\mathrm{kg\,m^{-3}}$. Consider first the impact of isolated snow particles whose diameter d is small compared to the sensor diameter D. In an idealized one-dimensional situation, we could use the theory of shock waves and the Rankine–Hugoniot curves for snow (Mellor, 1975, 1977; Bozhinskiy and Losev, 1998) to compute the particle diameters and velocities from the impact duration, τ, and the impulse on the sensor, I. Reality is significantly more complicated. First, particles are close to spherical and laterally unconfined except in the dense-flow layer. The expanding and then contracting shock front presumably takes longer to traverse the particle than in the one-dimensional problem, and the peak pressure is reduced. Secondly, the high stresses in the interior will soon disrupt the particle at the tip of the shock front. The debris continues to approach the sensor at roughly its original speed; if all of it lands on the sensor, the impulse (the integral of the force on the sensor over the duration of the impact) is still equal to the particle momentum, $I = mu$. However, a snow cone is likely to form on the sensor and to deflect particles (reducing I) or to cushion their impacts (increasing τ). Lacking more precise knowledge, we currently account for these effects with two adjustable parameters defined by $\alpha = mu/I$, $\alpha \geq 1$, and $\beta = d/(u\tau)$, $0.5 < \beta < 2$. Combining all of this we get

$$d = \left(\frac{6}{\pi}\alpha\beta\frac{I\tau}{\rho^{(p)}}\right)^{1/4} \text{ and } u = \left(\frac{6}{\pi}\frac{\alpha}{\beta^3}\frac{I}{\rho^{(p)}\tau^3}\right)^{1/4}. \quad (1)$$

β is seen to influence the velocity estimate quite significantly. In the present analysis we set $\alpha = \beta = 1.0$.

Particle–sensor interactions for large snow blocks

Experiments by Kawada (1983) and Abe and others (1992) show that a conical piece of compacted snow is rapidly punched out of a large block when it collides with the sensor. The observed initial pressure peak seems to be associated with the formation of this cone. The block disintegrates further and flows past the cone and sensor, the recorded pressures often being significantly below the initial peak; this means that little additional snow is compressed. Analyzing the data published by Abe and others (1992), we find the total impact duration to correspond quite precisely to the undisturbed time of passage of the block, $\tau = l/u$. Just as significantly, the recorded impulse agrees with the momentum of a snow column with the cross-section of the sensor to better than ±25%, except for a dense, refrozen sample with presumably much higher strength, where the measured impulse was about six times higher than expected from the other samples. We assume that snow blocks in a typical dry-snow avalanche correspond more closely to the unfrozen samples. It appears, though, that the snowballs in the wet-snow avalanche of 12 December 1998 had properties quite similar to those of the refrozen sample in the experiments of Abe and others (1992), whence the measured pressures far beyond the simple estimate $p \approx \rho u^2$.

Thus we take the diameter of a large block to be given by $u \approx d/\tau$, and the impulse by $I = \frac{\pi}{4}kD^2d\rho^{(p)}u$, where D is the sensor diameter and $k \approx 1.0$–1.25 (or up to ~10 in snow of high shear strength) accounts for the impact effects extending beyond the sensor. Solving for d and u,

$$d = \left(\frac{4}{\pi}\frac{I\tau}{kD^2\rho^{(p)}}\right)^{1/2} \text{ and } \quad u = \left(\frac{4}{\pi}\frac{I}{kD^2\rho^{(p)}\tau}\right)^{1/2}. \quad (2)$$

Corrections for excentrical impacts

Particles that are not small compared to the sensor will often collide excentrically with it (almost 90% of particles with diameter 5 cm!). This means that the impact duration is reduced from τ to τ' and that only a fraction of the particle momentum is intercepted by the sensor, I' instead of I. Thus particle size, velocity and density are severely underestimated if this effect is not accounted for. Unfortunately, the problem is rather intricate mathematically because the probability of excentric impacts rises quadratically with d and the excentricity is not known from the measurements. We outline a possible correction method here and apply it in section 5; significantly more work will be required to optimize the procedure.

We assume the particles to be spherical with diameter d and, integrating the intersection between a cylinder and a sphere, obtain $\tau' = \tau l/d$ from the length l of the cut surface

https://doi.org/10.3189/172756401781819409 Published online by Cambridge University Press

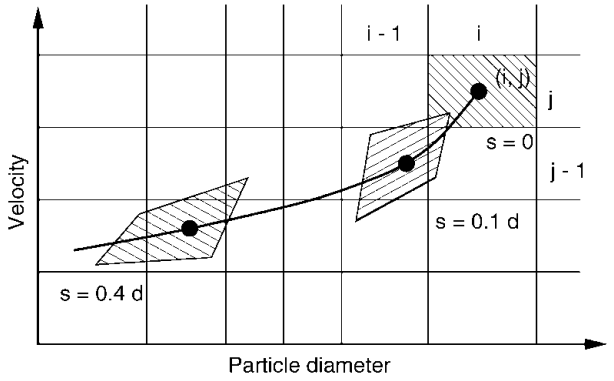

Fig. 3. Correction procedure for $N_{ij}(t)$ in the u-d plane. The images of class (i, j) for two different values of the excentricity s are shown. For each image determine the area fractions $r_{ij,i'j'}(s)$ it occupies within size class (i', j').

and $I' = Im'/m$ from the fraction of particle mass intercepted by the sensor. Denote the sensor diameter by D and the distance between particle and sensor centers in the sensor plane by s (excentricity); u is the true particle velocity. d' and u' denote the apparent diameter and velocity obtained from τ' and I' by means of Equation (1) or (2). For a particle of size d, the probability distribution of the excentricity is $p(s|d) = 8s/(D+d)^2$ with $0 \le s \le (D+d)/2$.

To make the problem tractable, we classify the particles in a finite number of size and velocity bins (i, j), $i = 1, 2, \ldots, i_{\max}$, $j = 1, 2, \ldots, j_{\max}$. Let $N_{ij}(t)$ be the true impact rate for true size/velocity class (i, j), and $\tilde{N}_{ij}(t)$ the impact rate attributed to (apparent) size/velocity class (i', j'). Assuming that the largest apparent diameters and velocities coincide with the true values — this will be satisfied if enough particles are detected — we may start from the largest and fastest particles in class $(i_{\max}, j_{\max})$ and transfer into this class all the particles of the same size and velocity with non-zero s that camouflage as smaller and slower particles in classes (i', j'). This procedure is repeated for decreasing i and j. More precisely, for a large number of s-values (step size Δs) the apparent boundaries of class (i, j) in the u-d plane and the fraction of the area of class (i', j') with $i' \le i$ and $j' \le j$ covered by the image of (i, j), $r_{ij,i'j'}(s)$ are computed (see Fig. 3). The contribution of (i', j') to (i, j) for this value of s is

$$\Delta N_{ij,i'j'}(t, s, \Delta s) = \tilde{N}_{ij}(t) r_{ij,i'j'}(s) \frac{p(s|d_i)}{P_0} \Delta s \qquad (3)$$

and is subtracted from $\tilde{N}_{i'j'}(t)$. P_0 is the integrated probability of s-values for which $d'(d, u|s)$ and $u'(d, u|s)$ remain within (i, j); we approximate it by the probability that the center of (i, j) will be mapped somewhere inside (i, j).

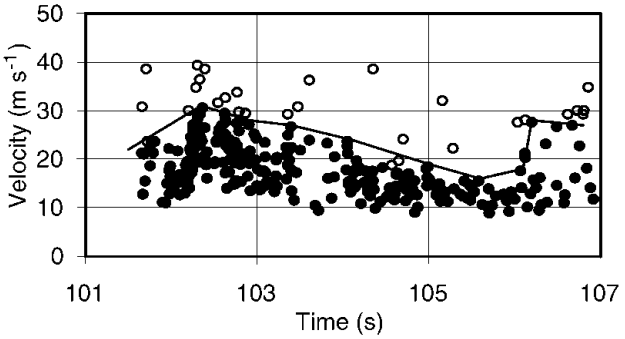

Fig. 4. Scatter plot of apparent particle velocities vs time at 3.0 m above ground, avalanche of 30 January 1999. Quasi-static pressure was removed before peak detection. Particles whose velocity was likely overestimated were discarded (open circles).

Determination of partial and total densities

The partial density of class (i, j) is obtained from

$$\rho_{ij}(t) = \frac{\pi}{6} d_i^3 \rho^{(p)} \frac{N_{ij}(t)}{u_j} \frac{4}{\pi (D + d_i)^2}, \qquad (4)$$

the last factor being the effective detector cross-section for particles of diameter d_i. The associated momentum flux is $\frac{2}{3} d_i^3 \rho^{(p)} N_{ij}(t)/(D + d_i)^2$. Similarly, the partial density of size class i and the total density are given by

$$\rho_i(t) = \sum_j \rho_{ij}(t) \text{ and } \rho(t) = \sum_i \rho_i(t). \qquad (5)$$

Substantial errors may be introduced if the size and velocity classes are chosen too wide. Furthermore, the total density obtained from Equation (5) does not take into account the contribution of particles too small to produce distinguishable impacts and is thus a lower limit on the true density of the flow.

5. DISTRIBUTION FUNCTIONS FOR PARTICLE SIZE AND VELOCITY

In a first step, single-particle impacts were selected for with rather restrictive criteria. Depending on the duration and impulse of the event, either Equation (1) or (2) was used to obtain particle size and velocity. Figure 4 presents the velocities thus obtained. Due to excentrical collisions, the true average velocities should be close to the upper limits of the scattered results in Figure 5; our estimate of the representative velocity is indicated by a line. These velocities are somewhat lower than the Doppler radar measurements. We will use them to

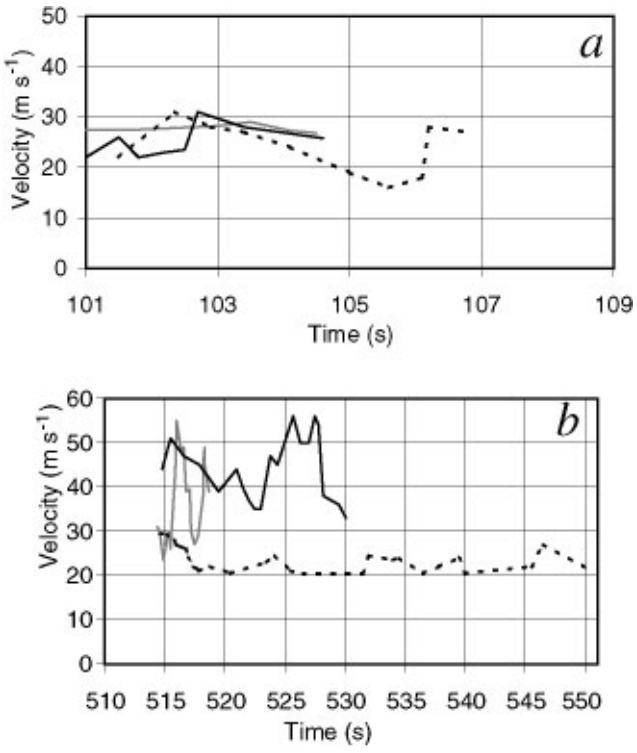

Fig. 5. Time evolution of apparent particle velocities at 3.0 m (dashed line), 3.9 m (full black line) and 7.0 m (gray line), avalanches of 30 January (a) and 10 February 1999 (b).

https://doi.org/10.3189/172756401781819409 Published online by Cambridge University Press

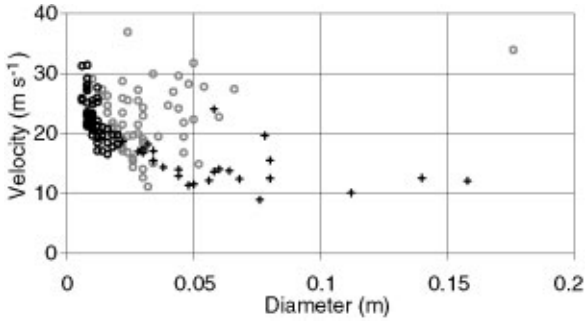

Fig. 6. Scatter plot of apparent particle velocity vs apparent particle diameter at 3.0 m (crosses), 3.9 m (gray circles) and 7.0 m (black circles). Avalanche of 30 January 1999, interval 101–102 s.

obtain density estimates from the impulse of particle clusters where single impacts cannot be distinguished. Differences in the velocity of large and small particles are recognizable on 30 January, but much less so on 10 February 1999 — presumably a consequence of the higher density and velocity of that event (Fig. 5).

The scatter plot in Figure 6 exemplifies, for a selected time interval, the correlations between velocity u and particle diameter d obtained at different heights in the flow. It is striking that almost all particles at 7 m height are $\mathcal{O}$(1 cm) on 30 January 1999; larger particles were found in the more violent 10 February 1999 avalanche. This finding is confirmed by the time evolution of the upper limit of particle size (see Fig. 7). With our present peak-detection algorithms and the relatively large sensors, the number of identifiable particles in each size class is rather low for obtaining precise velocity distribution functions. Thus Figure 8 should be considered a glimpse of the method's potential rather than a definitive result, but the finding that the small particles are generally faster than the larger ones is quite plausible.

Applying Equations (4) and (5) to the distribution functions, we obtain the time evolution of the partial densities, $\rho_{ij}(t)$ and $\rho_i(t)$, for size class i and velocity class j, as well as the total density of recognizable particles, $\rho_p(t)$. Figure 9 presents the results for the 10 February 1999 event at 7 m above ground; lower in the avalanche, many impact clusters could not be resolved into single particles by our present peak-detection algorithm. The last time interval in Figure 9 shows that very high densities occurred intermittently even at 7 m. Note, however, that only one particle was directly detected in this class; the contributions from non-central collisions amounted to 17 particles from smaller or slower classes. This shows both the paramount importance of the corrections and the sensitivity to errors and statistical fluctuations. The total mass flux and density during an interval Δt were estimated from the impulse on the sensors and the weighted average velocity obtained from the velocity distribution function. The main difficulty consists in choosing the adequate effective drag coefficient, depending on the particle-size distribution and the sensor size. As discussed by Schaerer and Salway (1980), McClung and Schaerer (1985) and Bozhinskiy and Losev (1998), the drag coefficient for quasi-stationary snow flow around small obstacles like our wedge and sensors might be in the range 1.0–1.2 (we used 1.1 in this case).

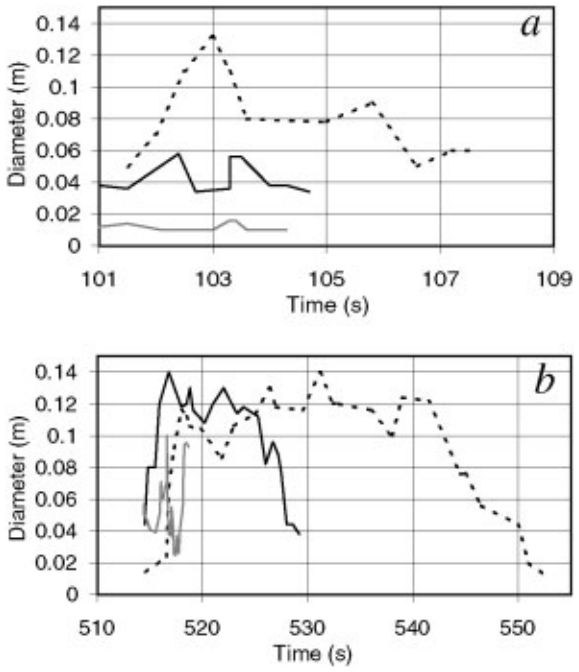

Fig. 7. Time evolution of apparent particle diameters at 3.0 m (dashed line), 3.9 m (full black line) and 7.0 m (gray line), avalanches of 30 January (a) and 10 February 1999 (b).

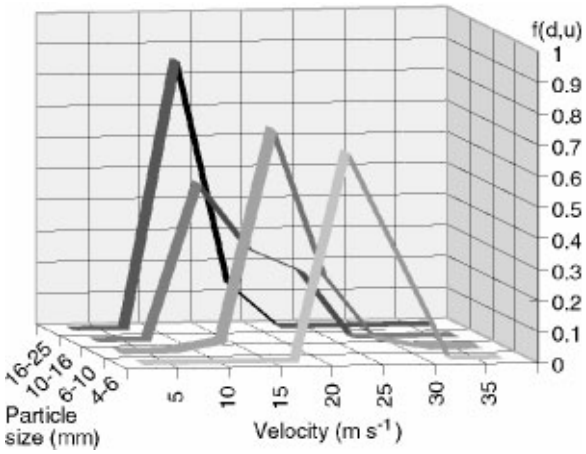

Fig. 8. Comparison of normalized velocity distribution functions for different particle-size classes, before corrections for excentric impacts. Avalanche of 30 January 1999, interval 103–103.5 s, sensor on mast at 7 m.

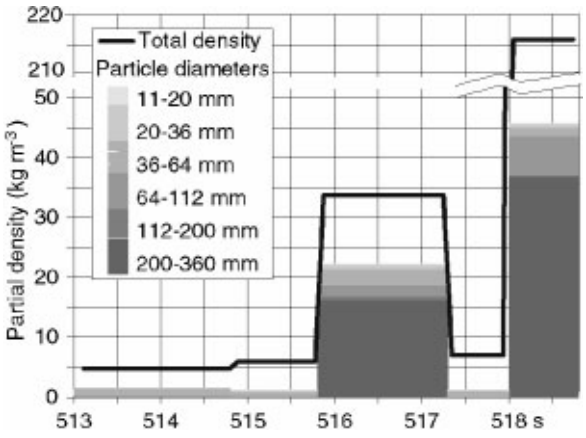

Fig. 9. Partial densities of different particle-size classes vs time. Avalanche of 10 February 1999, sensor at 7 m above ground. Widths of columns correspond to time-integration intervals. Estimated total density is plotted as line above partial densities.

https://doi.org/10.3189/172756401781819409 Published online by Cambridge University Press

6. CONCLUSIONS AND FUTURE WORK

Our present analysis of the 1999 pressure measurements at Vallée de la Sionne is to be considered exploratory and needs to be refined and expanded in many directions. Nevertheless, a number of qualitative or quantitative results have emerged and underline the great potential of this technique. The existence of the so-called saltation layer in dry-snow avalanches, consisting of snow blocks of widely different sizes, is clearly confirmed; this layer was absent in a slow wet-snow avalanche. Particles from 1 cm to about 50 cm in diameter were distinguished in measurements with load cells of diameter 10 cm. The same range of sizes was found by inspection of the avalanche deposits on the opposite slope. Between impacts, the pressure goes virtually to zero in the saltation layer, distinguishing it clearly from the dense flow underneath, where pressure fluctuations are observed on a background of high quasi-static pressure.

Much lower pressures than expected were found in the suspension layer, possibly due to formation of a streamlining "snow cap" on the sensor. Further analysis and possibly measurements based on different techniques will be required to clarify this important point.

Most significantly, our analysis shows that realistic partial densities, strongly varying in time from 1 to 45 kg m^{-3}, and distribution functions for particle size and velocity in the saltation layer can be extracted. They should prove particularly useful in developing and testing multi-layer models of mixed avalanches because the role of particle–particle collisions and the balance of forces can be assessed from the mean values and fluctuations of density and momentum. It should also be interesting to re-analyze older data from other test sites with the method proposed here.

However, much work is needed to refine the analysis methods: (i) Optimized criteria for peak detection will increase the statistical basis for the probability distribution functions and give more accurate results for the partial densities. (ii) The relations between impact duration, impulse, particle size and velocity need to be studied theoretically and in laboratory experiments. (iii) More advanced statistical methods are to be applied in correcting for excentric impacts, hopefully making the resulting densities less sensitive to fluctuations. (iv) Studying theoretically the interaction between a dense granular snow avalanche and a narrow obstacle should suggest ways of extracting relevant quantities like granular temperature from the data in the bottom layer. (v) Finally, we believe a more comprehensive, detailed and coherent picture of avalanche processes will emerge if the pressure measurements are extensively combined and confronted with data from other sensors, particularly the flow depths, velocity profiles and vertical fluctuation velocities from nearby FMCW/Doppler radars.

The exploratory analysis given here indicates that more sensors should be installed to obtain better vertical resolution and better statistics. Sensor diameter should be optimized between the conflicting requirements of high data rate and unambiguous reconstruction of single impacts. Two additional wedge-shaped support structures just below the two pairs of FMCW radars in the upper and lower track would allow comparison of flow regimes in different stages of the avalanche flow. It is important to replace the destroyed tubular mast and to design it for maximum suppression of high-frequency vibrations to facilitate measurements in the suspension layer. Installing pairs of capacitance probes on the mast at several heights would give the opportunity to measure pressure, density and velocity (from cross-correlations) directly and to clarify the open questions concerning PSA pressure. These conclusions confirm the proposals made by Harbitz and Issler (1998) for the instrumentation of a common European avalanche test site.

ACKNOWLEDGEMENTS

We wish to thank SLF's entire Vallée de la Sionne team — too numerous to list here — for their hard work, often performed under difficult conditions. Without all of them working together, these experiments would not have been possible. Special thanks go to M. Hartmann-Matsumura for her translation of Kawada (1983).

REFERENCES

Abe, O., H. Nakamura, A. Sato, N. Numano and T. Nakamura. 1992. Snow block impact pressures against a wall, a post and disks. *In Proceedings, Japan–U.S. Workshop on Snow Avalanche, Landslide, Debris Flow Prediction and Control, 30 September–2 October 1991, Tsukuba, Japan.* Tsukuba, Science and Technology Agency. National Research Institute for Earth Science and Disaster Prevention, 151–159.

Ammann, W. J. 1999. A new Swiss test-site for avalanche experiments in the Vallée de la Sionne/Valais. *Cold Reg. Sci. Technol.*, **30**(1–3), 3–11.

Bozhinskiy, A. N. and K. S. Losev. 1998. The fundamentals of avalanche science. *Eidg. Inst. Schnee- und Lawinenforsch. Mitt.* 55. (Translated from Russian by C. E. Bartelt.)

Dent, J. D., K. J. Burrell, D. S. Schmidt, M. Y. Louge, E. E. Adams and T. G. Jazbutis. 1998. Density, velocity and friction measurements in a dry-snow avalanche. *Ann. Glaciol.*, **26**, 247–252.

Dufour, F., U. Gruber, D. Issler, M. Schaer, N. Dawes and M. Hiller. Unpublished. Grobauswertung der Lawinenereignisse 1998/1999 im Grosslawinenversuchsgelände Vallée de la Sionne. Davos, Eidgenössisches Institut für Schnee- und Lawinenforschung. (Intern. Ber. 732.)

Gubler, H., M. Hiller, G. Klausegger and U. Suter. 1986. Messungen an Fliesslawinen. Zwischenbericht 1986. *Eidg. Inst. Schnee- und Lawinenforsch. Mitt.* 41.

Harbitz, C. B. and D. Issler. 1998. *Draft proposal for a co-ordinated European full-scale avalanche experiment.* Oslo, Norwegian Geotechnical Institute. (SAME Project Document D7, NGI Report 581220-2.)

Issler, D., *ed.* 1999. European avalanche test sites. Overview and analysis in view of coordinated experiments. *Eidg. Inst. Schnee- und Lawinenforsch. Mitt.* 59.

Kawada, K. 1983. [Impact pressure of snow block onto small circular plate.] *Seppyo, J. Jpn. Soc. Snow Ice*, **45**(2), 65–72. [In Japanese with English summary.]

Kawada, K., K. Nishimura and N. Maeno. 1989. Experimental studies on a powder-snow avalanche. *Ann. Glaciol.*, **13**, 129–134.

McClung, D. M. and P. A. Schaerer. 1985. Characteristics of flowing snow and avalanche impact pressures. *Ann. Glaciol.*, **6**, 9–14.

Mellor, M. 1975. A review of basic snow mechanics. *International Association of Hydrological Sciences Publication* 114 (Symposium at Grindelwald 1974 — *Snow Mechanics*), 251–291.

Mellor, M. 1977. Engineering properties of snow. *J. Glaciol.*, **19**(81), 15–66.

Nishimura, K., N. Maeno and K. Kawada. 1987. [Internal structures of large-scale avalanches revealed by a frequency analysis of impact forces.] *Low Temp. Sci., Ser. A* 46, 91–98. [In Japanese with English summary.]

Nishimura, K., N. Maeno, K. Kawada and K. Izumi. 1993. Structures of snow cloud in dry-snow avalanches. *Ann. Glaciol.*, **18**, 173–178.

Norem, H., T. Kvisterøy and B. D. Evensen. 1985. Measurement of avalanche speeds and forces: instrumentation and preliminary results of the Ryggfonn Project. *Ann. Glaciol.*, **6**, 19–22.

Schaerer, P. A. and A. A. Salway. 1980. Seismic and impact-pressure monitoring of flowing avalanches. *J. Glaciol.*, **26**(94), 179–187.

Vallet, J., U. Gruber and F. Dufour. 2001. Avalanche mass-balance measurements at Vallée de la Sionne. *Ann. Glaciol.*, **32** (see paper in this volume).